Nuclear Engineering and Technology 55 (2023) 3822–3830

Contents lists available at ScienceDirect

Nuclear Engineering and Technology

journal homepage: www.elsevier.com/locate/net

Original Article

Development of simultaneous multi-channel data acquisition system for large-area Compton camera (LACC)

Junyoung Lee [a, 1], Youngmo Ku [a, 1], Sehoon Choi [a], Goeun Lee [a], Taehyeon Eom [a], Hyun Su Lee [b], Jae Hyeon Kim [c], Chan Hyeong Kim [a, *]

[a] Department of Nuclear Engineering, Hanyang University, Seoul, 04763, South Korea
[b] Radioactivity Metrology Team, Korea Research Institute of Standards and Science, Daejeon, 34113, South Korea
[c] Radiation Utilization & Facilities Management Division, Korea Atomic Energy Research Institute, Jeongeup-si, Jeollabuk-do, 56212, South Korea

ARTICLE INFO

Article history:
Received 21 November 2022
Received in revised form
1 June 2023
Accepted 26 June 2023
Available online 27 July 2023

Keywords:
Compton imaging
Large-area Compton camera
Multi-channel data acquisition system
Digital signal processing
Field-programmable gate array

ABSTRACT

The large-area Compton camera (LACC), featuring significantly high detection sensitivity, was developed for high-speed localization of gamma-ray sources. Due to the high gamma-ray interaction event rate induced by the high sensitivity, however, the multiplexer-based data acquisition system (DAQ) rapidly saturated, leading to deteriorated energy and imaging resolution at event rates higher than 4.7×10^3 s^{-1}. In the present study, a new simultaneous multi-channel DAQ was developed to improve the energy and imaging resolution of the LACC even under high event rate conditions (10^4–10^6 s^{-1}). The performance of the DAQ was evaluated with several point sources under different event rate conditions. The results indicated that the new DAQ offers significantly better performance than the existing DAQ over the entire energy and event rate ranges. Especially, the new DAQ showed high energy resolution under very high event rate conditions, i.e., 6.9% and 8.6% (for 662 keV) at 1.3×10^5 and 1.2×10^6 s^{-1}, respectively. Furthermore, the new DAQ successfully acquired Compton images under those event rates, i.e., imaging resolutions of 13.8° and 19.3° at 8.7×10^4 and 10^6 s^{-1}, which correspond to 1.8 and 73 μSv/hr or about 18 and 730 times the background level, respectively.

1. Introduction

Compton imaging, which locates gamma-ray sources using Compton kinematics-based electronic collimation, has been studied for various applications in different fields including astrophysics [1–6], medical imaging [7–16], and nuclear security [17–23] since the principle was first proposed by Todd et al., in 1974 [24]. Since no mechanical collimation is required, most existing Compton cameras have been developed with small detectors in focusing on hand-held portability. The small size of these detectors, however, limits their imaging sensitivity (i.e., to 10^{-7}–10^{-6} for a ^{137}Cs source at 1 m distance), thereby requiring a considerable amount of time for localization of gamma-ray sources.

In our previous study [25], a high-sensitivity Compton camera, named the large-area Compton camera (LACC), was developed with large-size NaI(Tl) monolithic scintillators and photomultiplier tubes. The large size of the LACC made it possible to achieve an absolute imaging sensitivity of 3.4×10^{-5} for a ^{137}Cs point source at 1 m distance, which is more than ten-times-higher sensitivity than those of the existing Compton cameras. However, this high sensitivity induced a very high gamma-ray interaction event rate in the detectors, especially when imaging high-activity sources, thereby saturating the multiplexer-based data acquisition system (DAQ) of the LACC. This existing DAQ therefore was capable of handling only an event rate lower than 4.7×10^3 s^{-1}, which is equivalent to only two times of the natural background radiation level. Above this rate, the energy and imaging resolution deteriorated rapidly.

To remedy this defect, in the present study, we developed a new simultaneous multi-channel DAQ to improve the energy and imaging resolution of the LACC even under high event rate conditions (10^4–10^6 s^{-1}). For this purpose, a signal processing algorithm along with suitable operation parameters (i.e., trigger threshold and baseline window) were designed and implemented in the DAQ. The performance of the DAQ was evaluated in terms of energy and imaging resolution with several point sources under a wide range

* Corresponding author.
E-mail address: chkim@hanyang.ac.kr (C.H. Kim).
[1] These authors contributed equally to this paper.

https://doi.org/10.1016/j.net.2023.06.048

of event rate conditions, whose results were then compared with the corresponding values of the existing multiplexer-based DAQ.

2. Materials and methods

2.1. Large-area Compton camera (LACC)

Fig. 1 shows the LACC employed for evaluation of the newly developed DAQ. The LACC consists of two quad-type detectors called scatter and absorber and absorber detectors. Each detector consists of four monolithic NaI(Tl) scintillators (Scintitech, MA, USA) of large area (=14.6 × 14.6 cm^2) assembled in a 2 × 2 array. The thicknesses of scintillators for the scatter and absorber detectors are 2 and 3 cm, respectively, and the distance between the two detectors is 25 cm. Behind each scintillator, nine square-type photomultiplier tubes (PMTs) (R6764-01; Hamamatsu Photonics, Japan) each with a charge-sensitive preamplifier (τ = 1.23 μS) are placed in 3 × 3 array, being optically coupled to the scintillator with optical grease (BC-600, Saint-Gobain Crystals, OH, USA). The PMT (with a preamplifier) outputs a tail pulse of 800 ns rise time (from 1 to 99%). Each detector is enclosed individually within a dedicated shock-resistant housing of aluminum and stainless steel.

2.2. Simultaneous multi-channel data acquisition system (DAQ)

Fig. 2(a) shows the hardware of the simultaneous multi-channel DAQ developed in the present study, which consists of eight slave boards and one master board. The slave board comprises (1) nine high-speed (100 mega samples per second, = 10 ns/sample) 12-bit analog-to-digital converters (ADCs; ADS-4129, Texas Instruments, TX, USA) for digitizing individual PMT output signals and (2) a field-programmable gate array (FPGA; Arria V 5AGXMA5G4F31I5G, Intel, CA, USA), hereafter called a slave FPGA, for calculating the height and timing of a digitized pulse signal. The master board is composed of (1) an FPGA (Cyclone V 5CEBA7F31C7N, Intel, CA, USA), hereafter called a master FPGA, for collecting and analyzing the pulse data from slave boards and (2) a USB 3.0 module (EZ-USB, Infineon Technologies, Germany) for transferring the data to a personal computer. High-speed coaxial cables (HHSC-1-07-300-SU-SU, Samtec, IN, USA) are used for data communication between the slave and master boards. The power consumption of the developed DAQ system during operation is approximately 72 W (with an input voltage of 12 V and current of 6 A), which is comparable to that of a typical laptop computer and can be supplied by a small switching mode power supply.

Fig. 2(b) shows a schematic diagram of digital signal processing in the developed DAQ. During the operation of the LACC, the nine ADCs on each slave board individually digitize the nine PMT signals (corresponding to a single scintillator) with the speed of 100 mega samples per second. Simultaneously, the slave FPGA processes the digitized signals, determining the height and timing of incoming pulses, according to the following three algorithmic steps (see Fig. 3).

i) **Smoothing**: To reduce high-frequency noise, the incoming PMT signals are continuously smoothed by using a moving average method as shown in Fig. 3(a). The moving average window was set to 80 ns (8 samples), which is the maximum width that can be achieved with the finite operational resources of the slave FPGA. Note that the window is only 10% of the pulse rise time (800 ns), thus limiting the loss of energy (pulse height) resolution by over-smoothing.

ii) **Triggering**: To detect energy deposition by gamma-ray interaction events in a scintillator, the variation in the sum of the nine PMT signals (from a single scintillator) is monitored at each ADC sampling point by means of the difference between the sum signals at the current point and those at the 800 ns-earlier point (= rise time), as shown in Fig. 3(b). When the difference exceeds a predefined threshold level (= trigger threshold), the sampling point is determined as the pulse timing (t_p) for the event assuming that an energy deposition event occurred in the corresponding scintillator, and pulse height measurement for the nine input signals is triggered. Determination of the trigger threshold value will be discussed in Section 2.3.

iii) **Measuring of pulse height**: When triggered, the slave FPGA calculates the pulse heights for the nine PMT signals, as shown in Fig. 3(c). The pulse height measurement methodology implemented in this step facilitates the management of pile-up events. To manage the pile-up events, the pulse height is defined as the difference between the maximum and baseline level of the pulse signal, where the maximum level is the highest signal value within 800 ns after the pulse timing. Note that the baseline level is the average value of signals within a time window, named the baseline window (T_{bw}), which ranges from T_{bw} before the earlier point (t_p - 800 ns - T_{bw}) to the earlier point (t_p - 800 ns). Determination of the baseline window value also will be discussed in Section 2.3.

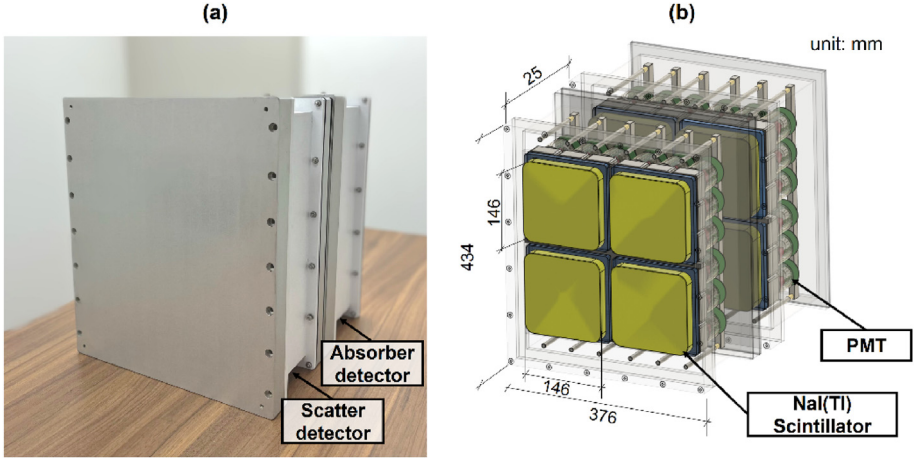

Fig. 1. (a) Picture and (b) 3D drawing of large-area Compton camera (LACC) employed in present study.

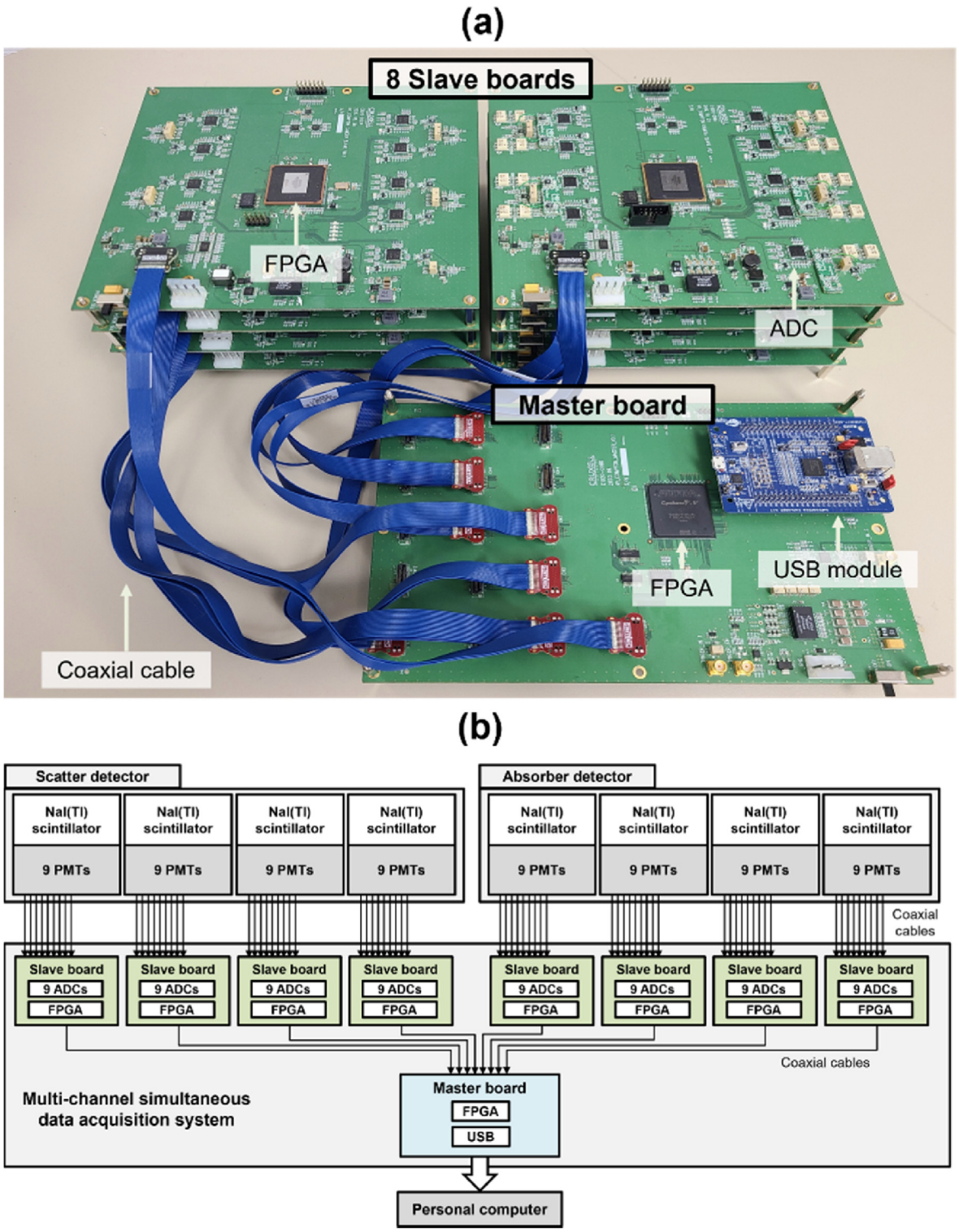

Fig. 2. (a) Simultaneous multi-channel data acquisition system (DAQ) and (b) schematic diagram of digital signal processing in DAQ.

The event data (i.e., pulse timing and height) obtained in the slave board are then immediately transmitted to the master board. In the master board, the master FPGA classifies the collected events into two categories: coincidence event (for Compton imaging) or single event (for nuclide identification) with a coincidence window (200 ns) which was calculated based on the time resolution (15.08 ns) of the quad-type detector evaluated in a previous research [26]. If another event is collected in the slave board that belongs to the other detector within a coincidence window (200 ns) from the pre-existing event (i.e., pulse timing), those two events are classified as coincidence events. Otherwise, the event is classified as a single event. The event classification and pulse height data are

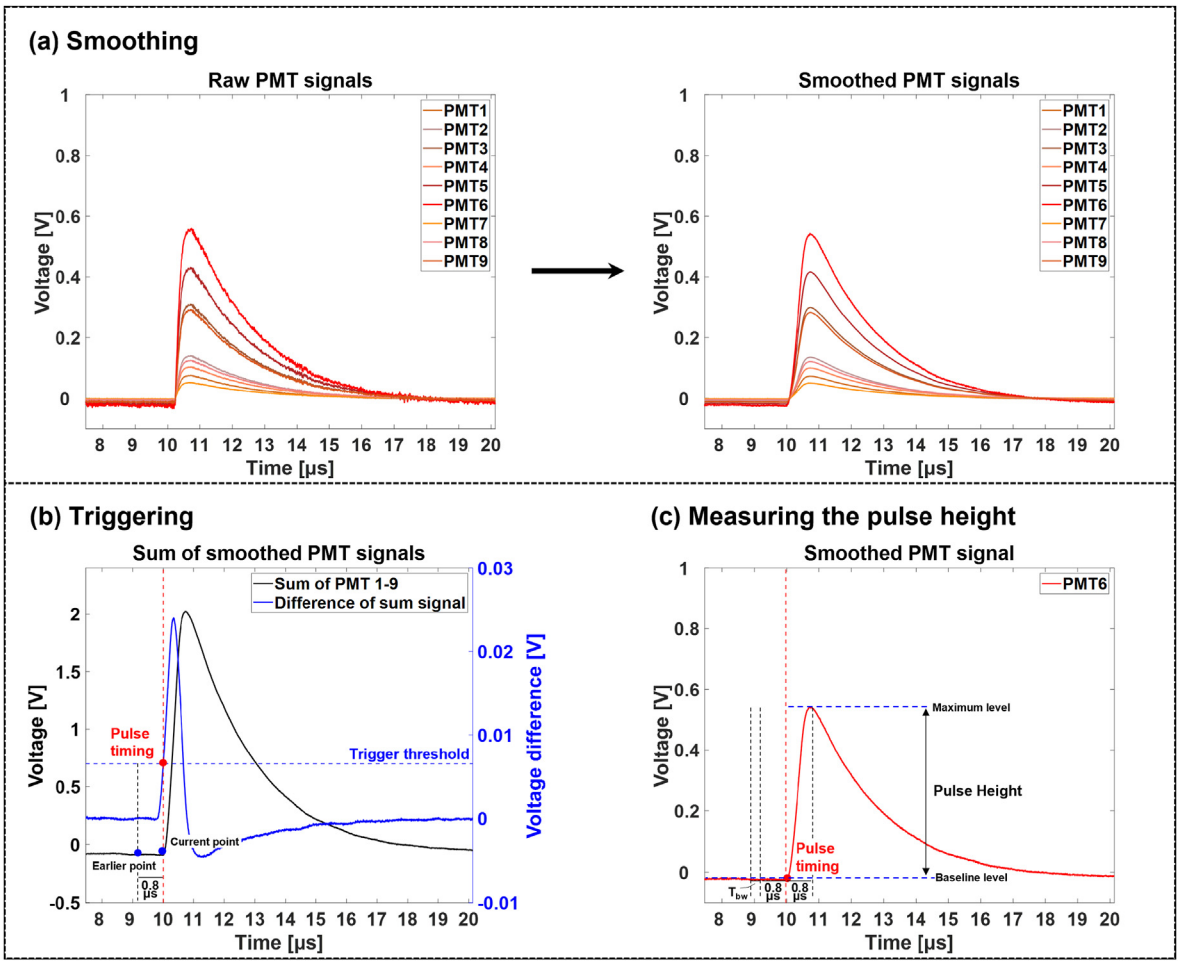

Fig. 3. Signal processing algorithm for determination of event timing and pulse height.

then transferred to the personal PC through the USB module.

2.3. Determination of operation parameters

In the present study, two operation parameters, i.e., trigger threshold and baseline window, were determined in the signal processing algorithm to achieve the maximum performance of the new DAQ. Considering the fact that the detection of the low energy photon is critical for Compton imaging especially for the events with small angle scattering at the scatter detector, the trigger threshold, which is equivalent to minimum measurable energy, should be lowered as far as possible; on the other hand, however, the random electrical noise should not account for a significant proportion of the total count. Therefore, in the present study, the trigger threshold was determined by evaluating the noise fraction, which is defined as the ratio between the number of counts caused by noise and by both noise and signal (= radiation interaction), for various trigger thresholds. Note that for conservative evaluation, the number of counts by signal was evaluated without introducing a gamma-ray source, thereby taking only the background radiation (dose rate ≈ 0.1 μSv/h) into account.

The baseline window is applied for reduction of statistical uncertainty in determining the baseline level. Adoption of the baseline window improves the energy resolution of the detector, but at the same time, it increases the signal processing time for a single pulse (= time required for triggering and measuring maximum pulse level), i.e., from 1600 ns to 1600 ns + T_{bw}, which may deteriorate detector throughput. Given those factors, the baseline window was determined by evaluating the energy resolution and signal processing time for five different windows (10, 20, 40, 80, and 160 ns) using 662 keV gamma rays from a ^{137}Cs source (activity = 7.12 μCi) located in front of the LACC at a 50 cm distance.

2.4. Performance evaluation

The performance of the new DAQ with the LACC was evaluated in terms of energy resolution, angular resolution measure (ARM), and Compton imaging resolution for detection of ^{241}Am, ^{22}Na, or

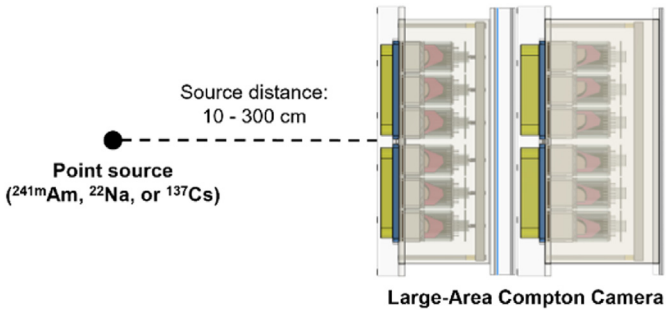

Fig. 4. Experimental setup to evaluate performance of data acquisition system (DAQ) with large-area Compton camera (LACC).

^{137}Cs point source located in front of the LACC (see Fig. 4). Note that the ARM is the distribution of the angular difference between the Compton scattering angle (θ_{Comp}) and the angle (θ_{Geom}) defined by the location of the gamma-ray source and interaction position [27]. The energy resolution was evaluated at (1) several energies (^{241}Am: 59.5, ^{133}Ba: 356, ^{137}Cs: 662, and ^{22}Na: 1275 keV) under a relatively low gamma-ray interaction event rate ($\approx 7.2 \times 10^3$ s^{-1}) and (2) several event rates ranging from 4.7×10^3 to 1.2×10^6 s^{-1} for 662 keV gamma rays (^{137}Cs point source). The ARM and the Compton imaging resolution were evaluated by acquiring Compton images at several different event rates ranging from 9.7×10^2 to 1.0×10^6 s^{-1} for 662 keV gamma rays (^{137}Cs point source) using the simple back-projection algorithm [28]. For all of the evaluations, the source activity and the distance from the source to the LACC varied to produce different event rate conditions, and hence also different dose rates. To observe the improvement of the new DAQ from the existing one, the performance of the existing one was evaluated under similar conditions. The experimental conditions for the new and existing DAQ are tabulated in Table 1. Note that the event rate and dose rate values in Table 1 are attributable only to the source, i.e., excluding background radiation, which were estimated using the Geant4 Monte Carlo simulation toolkit (ver. 10.06. p02) [29] and RADPRO Calculator® [30], respectively. Note that the event rate values were estimated as the sum of the counts from the four NaI(Tl) scintillators in the scatter detector, which means the event rate per NaI(Tl) scintillator is 1/4 of the value. The dose rate values were estimated at the center of the front surface of the scatter detector.

3. Results and discussion

3.1. Determination of operation parameters

Fig. 5 plots the results of the noise fraction evaluation to determine the trigger threshold. When the trigger threshold was set to 9 ADU (1 ADU ≈ 0.274 keV), the noise fraction was 80.4%. The noise fraction rapidly decreased with the threshold and reached down to 0.04% when the threshold was set to 108 ADU. This result shows that a high trigger threshold is desirable for noise suppression. As mentioned in Section 2.3, however, lowering the threshold is required for efficient Compton imaging in the context of low energy deposition by small angle scattering. Considering both the noise fraction and Compton imaging efficiency, the trigger threshold was determined to be 36 ADU, where the noise fraction (0.48%) was just below 1%. The determined threshold is equivalent to 9.9 keV energy, which allows for detection of energy deposition by Compton scattering with a small scattering angle (e.g., down to 8.8° for 662 keV). Note that the experimental condition was very conservative (i.e., the signal event rate was only at the background radiation level), and that the noise fraction will be much smaller in higher radiation fields with sources.

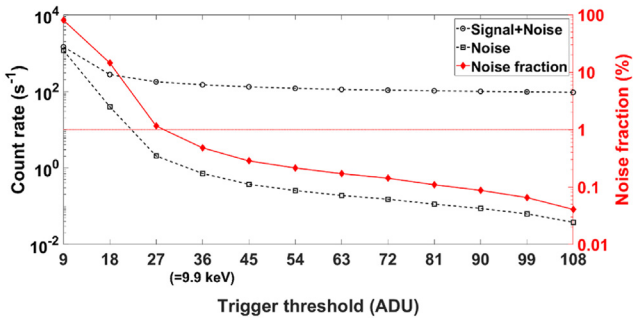

Fig. 5. Total (signal + noise) count rate, noise count rate, and noise fraction as evaluated for different trigger thresholds.

Fig. 6 plots the energy resolution of the new DAQ with the LACC for the 662 keV photopeak (^{137}Cs) and five different baseline windows (T_{bw}; 10, 20, 40, 80, and 160 ns). The energy resolution tended to improve with baseline windows from 10 ns to 40 ns, and the energy resolution improved from 7.5% to 6.9%. For larger baseline

Table 1
Experimental conditions for evaluation of performance of data acquisition system (DAQ) with large-area Compton camera (LACC).

	Existing DAQ						Developed DAQ					
	Experimental conditions				Event rate (s^{-1})	Dose rate (μSv/hr)	Experimental conditions				Event rate (s^{-1})	Dose rate (μSv/hr)
	Isotope	Energy (keV)	Activity (μCi)	Distance (cm)			Isotope	Energy (keV)	Activity (μCi)	Distance (cm)		
Energy resolution (for low count rate)	^{241}Am	59.5	10.94	50	4.7×10^3	6.4×10^{-3}	^{241}Am	59.5	10.94	50	4.7×10^3	6.4×10^{-3}
	^{133}Ba	356	4.63		3.8×10^3	3.2×10^{-2}	^{133}Ba	356	4.63		3.8×10^3	3.2×10^{-2}
	^{137}Cs	662	7.12		4.7×10^3	8.0×10^{-2}	^{137}Cs	662	7.12		4.7×10^3	8.0×10^{-2}
	^{22}Na	1275	4.27		7.2×10^3	1.8×10^{-1}	^{22}Na	1275	4.27		7.2×10^3	1.8×10^{-2}
Energy resolution (for different count rate)	^{137}Cs	662	7.12	50	4.7×10^3	8.0×10^{-2}	^{137}Cs	662	7.12	50	4.7×10^3	8.0×10^{-2}
				40	6.2×10^3	1.3×10^{-1}			80.50	50	4.8×10^4	9.0×10^{-1}
				30	6.9×10^3	2.2×10^{-1}			161.89	50	8.7×10^4	1.8×10^0
				20	1.1×10^4	5.0×10^{-1}			249.60	50	1.3×10^5	2.8×10^0
				10	2.5×10^4	2.0×10^0				30	2.4×10^5	7.9×10^0
	–			–	-	-				10	8.8×10^5	7.1×10^1
	–			–	-	-				5	1.2×10^6	2.8×10^2
Angular resolution measure (ARM)	^{137}Cs	662	7.12	300	9.7×10^2	2.2×10^{-3}	^{137}Cs	662	7.12	300	9.7×10^2	2.2×10^{-3}
				100	2.9×10^3	2.0×10^{-2}				50	4.7×10^3	8.0×10^{-2}
				50	4.7×10^3	8.0×10^{-2}			80.50	20	4.8×10^4	9.0×10^{-1}
				20	1.1×10^4	5.0×10^{-1}			161.89	50	8.7×10^4	1.8×10^0
				10	2.5×10^4	2.0×10^0			249.60	50	1.3×10^5	2.8×10^0
	–			–	-	-				30	2.4×10^5	7.9×10^0
	–			–	-	-			2334.54	30	1.0×10^6	7.3×10^1
Imaging resolution	^{137}Cs	662	7.12	300	9.7×10^2	2.2×10^{-3}	^{137}Cs	662	7.12	300	9.7×10^2	2.2×10^{-3}
				10	2.5×10^4	2.0×10^0			161.89	50	8.7×10^4	1.8×10^0
			2334.54	30	1.0×10^6	7.3×10^1			2334.54	30	1.0×10^6	7.3×10^1

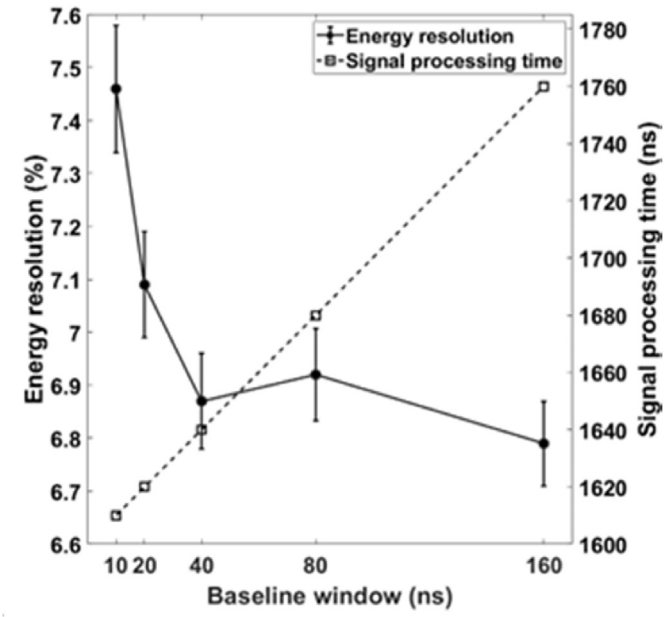

Fig. 6. Energy resolution of large-area Compton camera (LACC) with new data acquisition system (DAQ) for 662 keV (^{137}Cs) and five different baseline windows: 10, 20, 40, 80, and 160 ns.

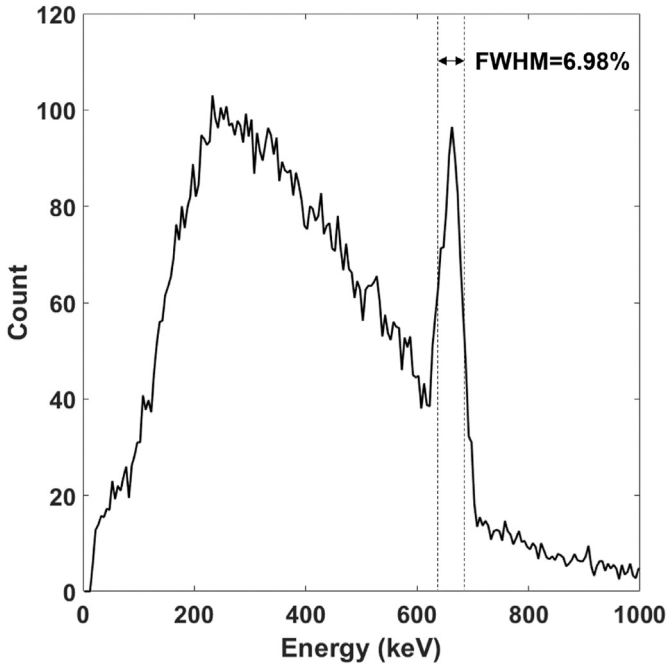

Fig. 7. Summed energy spectrum with new data acquisition system for ^{137}Cs. The measured energy resolution of 662 keV is 6.98% (FWHM).

windows, on the other hand, no significant improvement in the energy resolution was observed. Because the increased signal processing time with the baseline window may reduce the throughput of signal processing (as mentioned in Section 2.3), the baseline window was determined as 40 ns, and thus the signal processing time for a single pulse as 1640 ns? The determined baseline window was applied for both scatter and absorber detector, resulting in energy resolution (for 662 keV photopeak) comparable to each other (6.9% and 6.8%, respectively). As shown in Fig. 7, the energy resolution of the summed energy spectrum (i.e., acquired by the summation of scatter and absorber detector energy in coincidence event), which is required for Compton imaging, was evaluated as 6.98%, showing that the energy estimation performance of LACC is as good as most commercial detectors.

3.2. Performance evaluation of data acquisition system (DAQ)

Fig. 8 plots the energy resolution of the LACC scatter detector with the new and existing DAQs evaluated for 59.5, 356, 662, and 1275 keV peaks (^{241}Am, ^{133}Ba, ^{137}Cs, ^{22}Na) and relatively low gamma-ray interaction event rates (3.8×10^3–7.2×10^3 s^{-1}). For all of the energies, the new DAQ showed higher energy resolution (18.1, 8.5, 6.8, and 5.2%) than the existing DAQ (26.2, 9.6, 7.5, and 5.8%). This improvement may be attributed to two reasons: (a) direct transfer of the output from the PMT to the ADC and (b) improved algorithm for pulse height measurement. In the existing DAQ, the output from the PMT passes through several components including the shaping amplifier, sample and holder, and multiplexer before entering the ADC. In addition, the system records the maximum voltage of the input pulse as the pulse height without considering the baseline level. As a result, this method can lead to a deterioration in precision when pulses are piled up. Unlike the existing DAQ, the new DAQ directly collects PMT output signal by ADC, thereby immunizing the signal against analog noises promptly after digitization, and the developed DAQ precisely measure the maximum voltage of input pulse by employing the improved algorithm for pulse height measurement (e.g., smoothing, triggering, measuring of pulse height). The result showed that the energy resolution of the LACC scatter detector with the new DAQ (6.8% for 662 keV) was even comparable to commercial NaI(Tl) scintillation detectors (typically 6.5% for 662 keV) [31], even though the geometry of the LACC scatter detector is less desirable for high energy resolution (i.e., the light from a scintillator is converted to electrons and amplified by the nine different PMTs, which are not ideally cross-calibrated). The improved energy resolution of the LACC will be favorable not only for nuclide identification by gamma spectroscopy, but also for Compton imaging, by allowing for more precise scattering angle calculation.

Fig. 9 plots the energy resolutions of the new and existing DAQs evaluated for the 662 keV photopeak (^{137}Cs) under different event rate conditions ranging from 4.7×10^3 to 1.2×10^6 s^{-1}. The energy resolution with the existing DAQ was 7.5% at the lowest event rate, and rapidly deteriorated as the event rate increased, ebbing to 15.7% at an event rate of only 2.5×10^4 s^{-1}. Above this event rate (2.5×10^4 s^{-1}), the energy resolution of the existing DAQ could not be evaluated due to the incapability of measuring the pile-up pulses. The new DAQ, on the other hand, showed improved energy resolution (= 6.9%) at even 1.3×10^5 s^{-1} event rate. When the event rate was higher than 1.3×10^5 s^{-1}, the energy resolution started to slightly deteriorate, reaching 8.6% at 1.2×10^6 s^{-1}, due to the pile-up effect at the high event rate. It should be noted that the baseline calculation method employed for estimating the baseline exhibited limitations at high count rates, resulting in an incomplete discrimination of the pile-up pulses. Nevertheless, it is noteworthy that despite the slight degradation in energy resolution, the LACC with the new DAQ still operated at the 1.2×10^6 s^{-1} event rate, which corresponds to dose rate of 283 μSv/h (i.e., 2830 times the background dose rate (0.1 μSv/h)) [32].

Fig. 10(a) plots the ARM of LACC with the new and existing DAQs

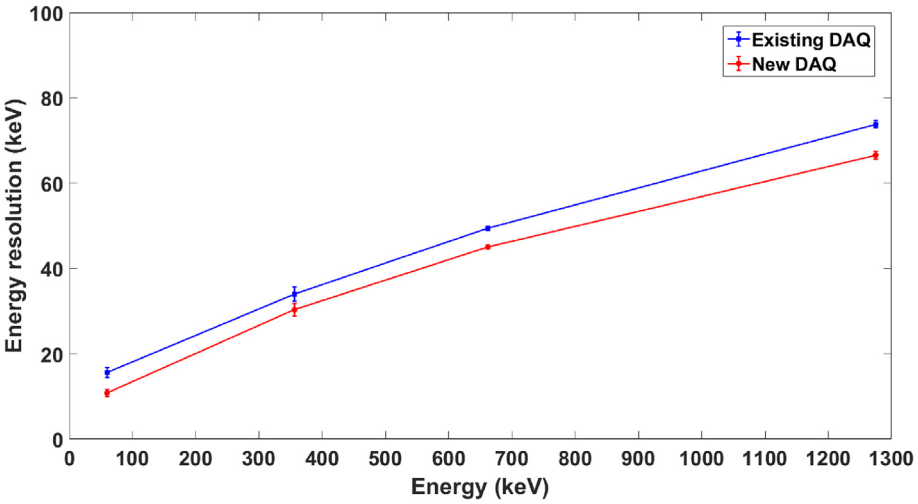

Fig. 8. Energy resolution of large-area Compton camera (LACC) (scatter detector) with new and existing data acquisition systems (DAQs) evaluated for 59.5, 356, 662, and 1275 keV peaks under low event rate conditions (3.8×10^3–7.2×10^3 s^{-1}).

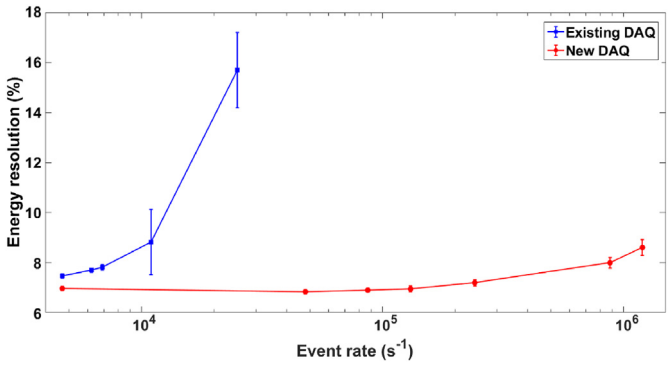

Fig. 9. Energy resolutions of new and existing data acquisition systems (DAQs) evaluated for 662 keV photopeak (^{137}Cs) under different event rate conditions ranging from 4.7×10^3 to 1.2×10^6 s^{-1}.

evaluated for the 662 keV photopeak (^{137}Cs) under different event rate conditions ranging from 9.7×10^2 to 10^6 s^{-1}. At event rates lower than 4.7×10^3 s^{-1}, the DAQs showed similar ARMs; the new DAQ (13.7–14.0°) showed a slightly improved ARM relative to that of the existing DAQ (14.2–14.3°). At event rates higher than 10^4 s^{-1}, however, the ARM of the existing DAQ sharply increased, reaching 24° at the 2.5×10^4 s^{-1} event rate, whereas that of the new DAQ was maintained below 15° up to the 2.4×10^5 s^{-1} event rate. When the event rate was higher than 2.4×10^5 s^{-1}, the ARM with the new DAQ also began to deteriorate but remained under 16.7° even up to the highest event rate (10^6 s^{-1}).

Fig. 10(b) shows Compton images acquired with the new and existing DAQs for the 662 keV photopeak (^{137}Cs) under different event rate conditions, which are marked with parenthesized case numbers referencing the event rates in Fig. 10(a). The acquisition time was 60 s for each case. When the event rate was very low ($\approx 9.7 \times 10^2$ s^{-1}, cases 1 and 4), in which case the dose rate at the location of the camera was only about 2% of the background dose rate (= 0.002 μSv/h), the new and existing DAQs showed similar Compton image qualities in terms of image resolution, i.e., 13.1° and 13.2°, respectively. Under the medium event rate conditions ($\approx 2.5 \times 10^4$ and 8.7×10^4 s^{-1}, cases 2 and 5), however, the imaging resolution of the existing DAQ was significantly degraded to 24.9° at the 2.5×10^4 s^{-1} event rate (cases 2), while that of the new DAQ was maintained at 13.8° at the 8.7×10^4 s^{-1}, which corresponds to dose rate of 1.8 μSv/h (~18 times the background dose rate). When the event rate was very high ($\approx 10^6$ s^{-1}, cases 3 and 6), in which case the dose rate at the location of the camera is 73 μSv/h (~730 times the background dose rate), the imaging resolution of the existing DAQ could not be evaluated (the source was not localized), whereas only small degradation of imaging resolution (i.e., to 19.3°) was observed with the new DAQ.

4. Conclusion

In the present study, a simultaneous multi-channel data acquisition system (DAQ) was newly developed to improve the energy and imaging resolution of the large-area Compton camera (LACC), especially under high gamma-ray interaction event rates. For this purpose, a signal processing algorithm along with suitable operation parameters (i.e., trigger threshold and baseline window) were designed and implemented in the DAQ. The optimized operation parameters were empirically determined through experiments. The performance of the new DAQ was then evaluated in terms of energy and imaging resolution using several point sources under a wide range of event rate conditions. Over the entire energy and event rate ranges evaluated in the present study, the new DAQ demonstrated better performance than the existing DAQ. Especially, the new DAQ showed high energy resolution (for 662 keV) even under very high event rate conditions, i.e., 6.9% for 1.3×10^5 s^{-1} and 8.6% for 1.2×10^6 s^{-1}, whereas the existing DAQ could not even be evaluated due to its incapability of measuring pile-up pulses. Furthermore, the new DAQ successfully acquired Compton images under the same event rate conditions, i.e., imaging resolutions of 13.8° and 19.3° for 8.7×10^4 and 10^6 s^{-1}, respectively, which correspond to 1.8 and 73 μSv/hr of the dose rates at the camera location or about 18 and 730 times the background radiation level.

Declaration of competing interest

The authors declare that they have no known competing financial interests or personal relationships that could have appeared to influence the work reported in this paper.

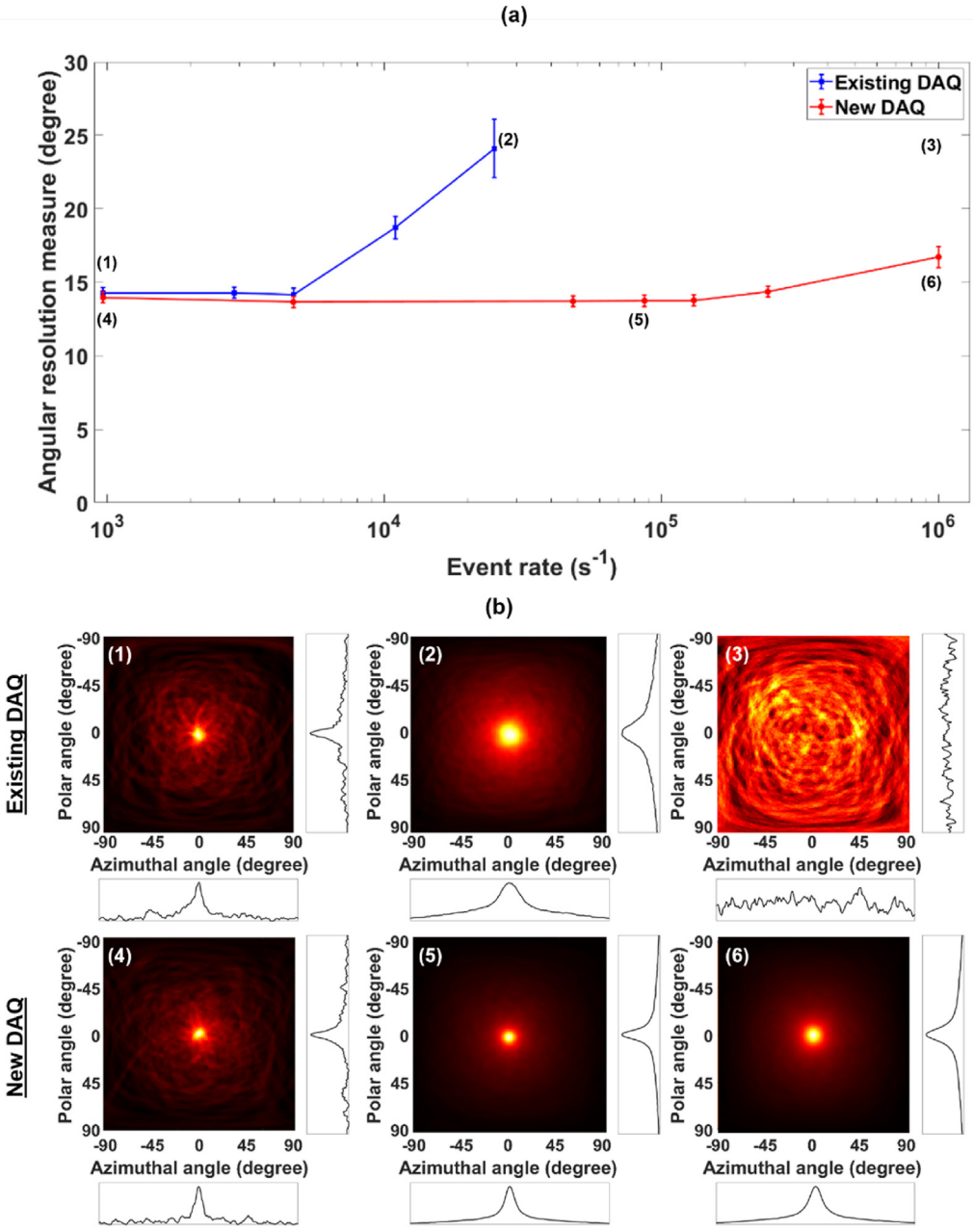

Fig. 10. (a) Angular resolution measure (ARM) and (b) Compton images acquired by large-area Compton camera (LACC) with new and existing data acquisition systems (DAQs) using 662 keV photopeak (^{137}Cs) under different event rate conditions ranging from 9.7 × 10^2 to 10^6 s^{-1}.

Acknowledgements

This research was supported by Field-oriented Technology Development Project for Customs Administration through National Research Foundation of Korea (NRF) funded by the Ministry of Science & ICT and Korea Customs Service (NRF-2021M3I1A1097895), and additionally, by the National Research Foundation of Korea (NRF) grant funded by the Ministry of Science & ICT (NRF-2019M2D2A1A02059814).

References

[1] H. Bloemen, et al., COMPTEL imaging of the galactic disk and the separation of diffuse emission and point sources, Astrophys. J. Suppl. 92 (1994) 419–423.
[2] S.C. Kappadath, et al., The preliminary cosmic diffuse gamma-ray spectrum from 800keV to 30MeV measured with COMPTEL, Astron. AstroPhys. Suppl. 120 (1996) 619–622.
[3] V. Schonfelder, et al., Instrument description and performance of the imaging gamma-ray telescope COMPTEL aboard the Compton gamma-ray observatory, Astrophys. J. Suppl. 86 (1993) 657–692.
[4] H. Steinle, et al., COMPTEL observations of centaurus a at MeV energies in the years 1991 to 1995, Astron. Astrophys. 330 (1998) 97–107.
[5] S.E. Boggs, The advanced Compton telescope mission, N. Astron. Rev. 50 (7) (2006) 604–607.
[6] V. Schonfelder, et al., Instrument description and performance of the imaging gamma-ray telescope COMPTEL aboard the Compton Gamma-Ray Observatory, Astrophys. J. Suppl. (1993).
[7] M. Singh, An electronically collimated gamma camera for single photon emission computed tomography. Part I: theoretical considerations and design criteria, Med. Phys. 10 (4) (1983) 421–427.
[8] M. Singh, et al., An electronically collimated gamma camera for single photon emission computed tomography. Part II: image reconstruction and preliminary experimental measurements, Med. Phys. 10 (4) (1983) 428–435.
[9] J.B. Martin, et al., A ring Compton scatter camera for imaging medium energy gamma rays, IEEE Trans. Nucl. Sci. 40 (4) (1993) 972–978.

[10] J.W. Leblanc, et al., C-SPRINT: a prototype Compton camera system for low energy gamma ray imaging, IEEE Trans. Nucl. Sci. 45 (3) (1998) 943–949.
[11] M. Yamaguchi, et al., Development of head module for multi-head Si/CdTe Compton camera for medical applications, Nucl. Instrum. Methods Phys. Res. Sect. A Accel. Spectrom. Detect. Assoc. Equip. 648 (2011) S2–S7.
[12] P.F. Bloser, et al., The MEGA project: science goals and hardware development, N. Astron. Rev. 50 (7) (2006) 619–623.
[13] G. Kanbach, et al., The MEGA project, N. Astron. Rev. 48 (1) (2004) 275–280.
[14] A. Zoglauer, et al., Data analysis for the MEGA prototype, N. Astron. Rev. 48 (1) (2004) 231–235.
[15] E. Draeger, et al., 3D prompt gamma imaging for proton beam range verification, Phys. Med. Biol. 63 (3) (2018), 035019.
[16] Kenji Shimazoe, et al., Development of simultaneous PET and Compton imaging using GAGG-SiPM based pixel detectors, Nucl. Instrum. Methods Phys. Res. Sect. A Accel. Spectrom. Detect. Assoc. Equip. 954 (2020), 161499.
[17] C.G. Wahl, et al., The Polaris-H imaging spectrometer, Nucl. Instrum. Methods Phys. Res. Sect. A Accel. Spectrom. Detect. Assoc. Equip. 784 (2015) 377–381.
[18] A. Harayama, et al., "A portable Si/CdTe Compton camera and its applications to the visualization of radioactive substances," Nucl. Instrum. Methods Phys. Res. Sect. A Accel. Spectrom. Detect. Assoc. Equip., vol. 787, pp. 207–211.
[19] J. Kataoka, et al., Handy Compton camera using 3D position-sensitive scintillators coupled with large-area monolithic MPPC arrays, Nucl. Instrum. Methods Phys. Res. Sect. A Accel. Spectrom. Detect. Assoc. Equip. 732 (2013) 403–407.
[20] M.L. Galloway, et al., Status of the high efficiency multimode imager, in: Nuclear Science Symposium and Medical Imaging Conference (NSS/MIC), 2012, pp. 1290–1293.
[21] K. Vetter, et al., Advanced concepts in multi-dimensional radiation detection and imaging, in: Proceedings of International Symposium on Radiation Detectors and Their Uses (ISRD2016), 2016, https://doi.org/10.7566/JPSCP.11.070001.
[22] J.G. Dreyer, et al., "Next Generation Germanium Systems for Safeguards Applications," No. LLNL-CONF-660195, Lawrence Livermore National Laboratory (LLNL), Livermore, CA, 2014.
[23] Jianyong Jiang, et al., A prototype of aerial radiation monitoring system using an unmanned helicopter mounting a GAGG scintillator Compton camera, J. Nucl. Sci. Technol. 53 (7) (2016) 1067–1075.
[24] R.W. Todd, et al., A proposed gamma camera, Nature 251 (1974) 132–134.
[25] Y. Kim, et al., Large-area Compton camera for high-speed and 3-D imaging, IEEE Trans. Nucl. Sci. 65 (11) (2018) 2817–2822.
[26] H. Lee, Large-area Hybrid Gamma Imager: Fast Localization of Gamma-Ray Sources" PhD Diss, Hanyang University, 2021.
[27] S. Watanabe, et al., A Si/CdTe semiconductor Compton camera, IEEE Trans. Nucl. Sci. 52 (2005) 2045–2051.
[28] Y. Kim, W. Lee, Development of a virtual frisch-grid CZT detector based on the array structure, Journal of Radiation Protection and Research 45 (1) (2020) 35–44.
[29] S. Agostinelli, et al., GEANT4-a simulation toolkit, Nucl. Instrum. Methods A 506 (3) (2003) 250–303.
[30] McGinnis Ray RADPRO calculator® 2015, available at, www.radprocalculator.com/Gamma.aspx.
[31] N. Demir, Z.N. Kuluöztürk, Determination of energy resolution for a NaI(Tl) detector modeled with FLUKA code, Nucl. Eng. Technol. 53 (11) (2021) 3759–3763.
[32] H. Lee, et al., Development and performance evaluation of large-area hybrid gamma imager (LAHGI), Nucl. Eng. Technol. 53 (8) (2021) 2640–2645.